Supporting Information for "Bayesian multi-model estimation for fault slip distribution: the effect of prior constraints in the estimation for slow slip events beneath the Bungo Channel, southwest Japan"

R. Agata[1], R. Nakata[2], A. Kasahara[3], Y. Yagi[4], Y. Seshimo[5], S. Yoshioka[6,5], T. Iinuma[1]

[1]Japan Agency for Marine-Earth Science and Technology, 3173-25 Showa-machi, Kanazawa-ku, Yokohama 236-0001, Japan

[2]Graduate School of Science, Tohoku University, 6-6 Aramaki-aza-aoba, Aoba-ku, Sendai 980-8578, Japan

[3]Independent researcher

[4]Faculty of Life and Environmental Sciences, University of Tsukuba, 1-1-1 Tennodai, Tsukuba-shi, Ibaraki 305-8572, Japan

[5]Department of Planetology, Graduate School of Science, Kobe University, 1-1 Rokkodai-cho, Nada-ku, Kobe, Hyogo, Japan, 657-8501, Japan

[6]Research Center for Urban Safety and Security, Kobe University, 1-1 Rokkodai-cho, Nada-ku, Kobe 657-8501, Japan

Contents of this file

Introduction This Supporting Information contains additional results of the numerical experiments and the estimations using actual geodetic data. The posterior PDFs of the underground structure estimated for SM_{smooth} in the numerical experiment are shown in

Figures S1. The choice of the grid spacing using an information criterion is discussed in Text S1 and Table S1. The residual displacements plotted for the estimation for the 2010 and 2018 L-SSE are shown in Figure S2. Calculation of the slip direction based on the estimation results for the rake deviation is presented in Text S2 and Figure S3. The re-sampled samples for the prior PDF that from those obtained as the posterior PDF estimated for the 2010 L-SSE are shown in Figure S4. The spatial distributions of the number of tremor before and during the period of L-SSE are compared in Figure S5. The spatial distributions of $\Delta\tau$, the shear stress change on the fault, calculated by using the results of BMMFSE the smoothing model are compared in Figure S6.

Text S1.

In fully Bayesian inference of slip distribution without introducing regularization, a significant dependence of the estimation result on the choice of the grid pattern has been reported (Minson et al., 2013). Therefore, objective and quantitative determination of the grid pattern, which is classified as a "model selection" problem, is desirable. Minimization of minus logarithmic marginalized likelihood, or also referred to as model evidence, enables an objective model selection in Bayesian inference (see Bishop (2006)). We use the widely applicable Bayesian information criterion (WBIC) (Watanabe, 2013), which calculates the minus logarithm marginalized likelihood approximately, obtained in the estimations for the 2010 L-SSE to determine the spacing of the grid. Thus, the horizontally regular grid with a spacing of 16 km is chosen as mentioned in Section 3.3. Table S1 compares WBIC the various grid spacings.

Text S2.

We consider the rake deviation of the slip from the direction opposite to subduction (i.e., 125° in the north-based azimuth) as an unknown in the estimation. We obtain the random samples from the posterior PDF of the rake deviation. To compare the result with the slip direction projected to the horizontal plane estimated for the same events in Yoshioka et al. (2015) , we perform a conversion from the rake deviation to slip direction. For this purpose, we need to specify the normal vector of the fault plane to define the rake angle. Because we consider a 3D plate boundary geometry, the normal vector varies depending on the location of the fault. As a representative normal vector of the main rupture area, we chose the one defined at 132.364°E and 33.026°N on the Nakanishi model (Nakanishi et al., 2018). Figure S3 shows the histograms for the slip direction in the north-based azimuth calculated based on the rake deviation from the 125° azimuth estimated for the 2010 and 2018 L-SSE based on the representative normal vector.

References

Bishop, C. M. (2006). *Pattern recognition and machine learning*. springer.

Kano, M., Kato, A., & Obara, K. (2019). Episodic tremor and slip silently invades strongly locked megathrust in the Nankai Trough. *Scientific reports*, *9*(1), 1–8.

Minson, S., Simons, M., & Beck, J. (2013). Bayesian inversion for finite fault earthquake source models I–Theory and algorithm. *Geophysical Journal International*, *194*(3), 1701–1726.

Nakanishi, A., Takahashi, N., Yamamoto, Y., Takahashi, T., Citak, S. O., Nakamura, T., ... Kaneda, Y. (2018). Three-dimensional plate geometry and P-wave velocity models of the subduction zone in SW Japan: Implications for seismogenesis. *Geology and Tectonics of Subduction Zones: A Tribute to Gaku Kimura*, *534*, 69.

Watanabe, S. (2013). A widely applicable bayesian information criterion. *Journal of Machine Learning Research*, *14*(Mar), 867–897.

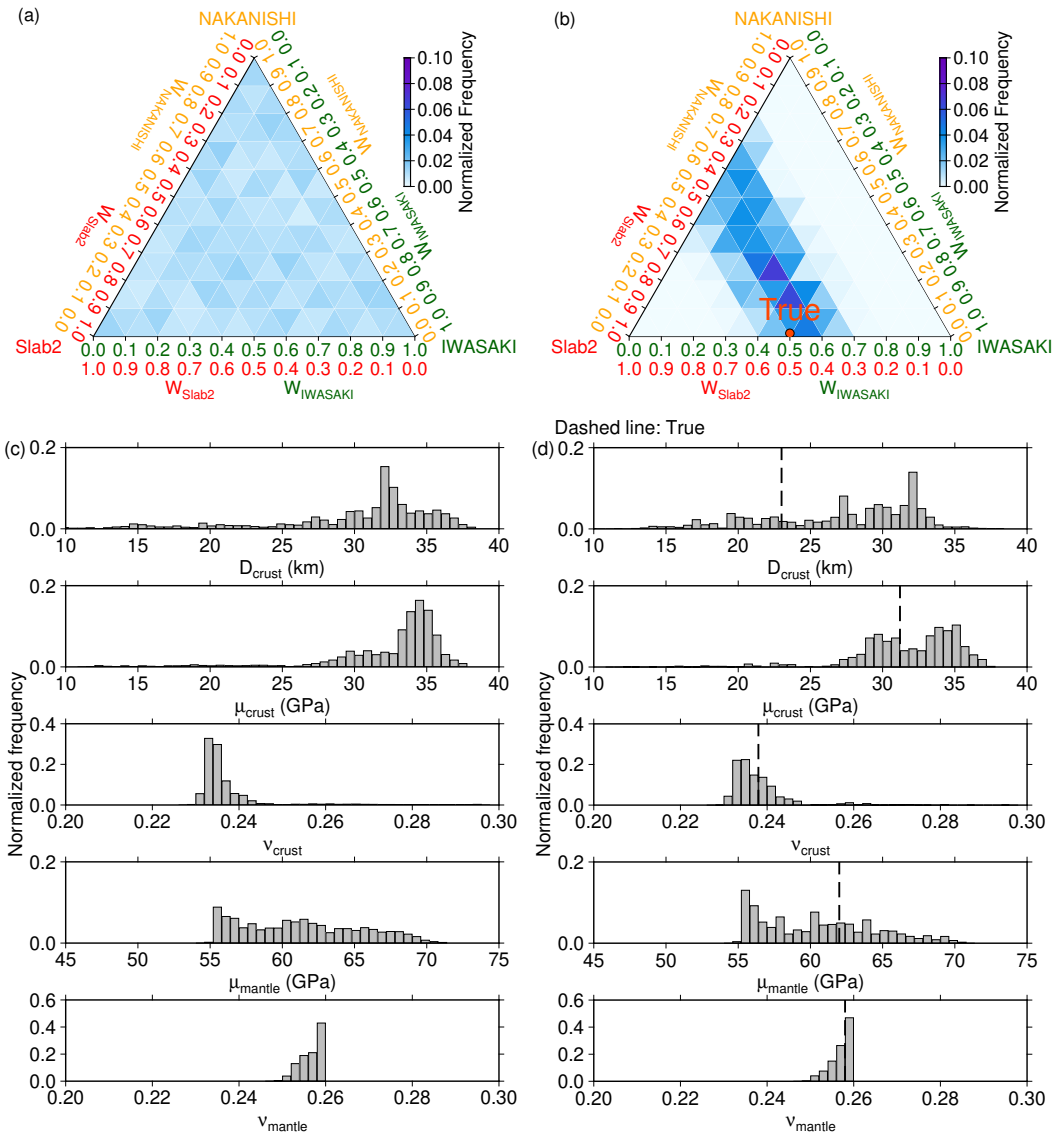

Figure S1. Comparison of the prior and posterior PDF of the underground structure in the numerical experiment for SM_{smooth}. The ternary plots for (a) the prior and (b) posterior PDF of the plate boundary geometry model. The histograms for (c) the prior and (d) posterior PDF of the elastic structure.

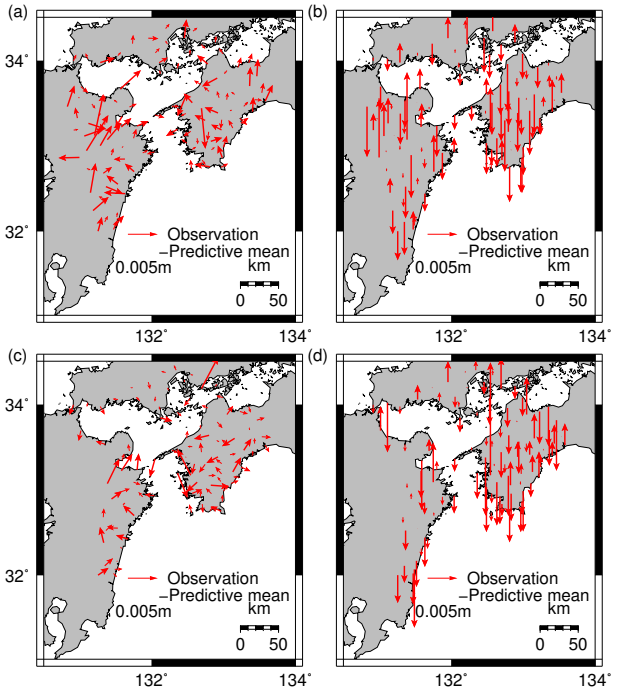

Figure S2. Residual (observation subtracted by mean of predictive mean) displacement in the estimation for the 2010 ((a) for the horizontal and (b) for the vertical component) and 2018 L-SSE ((c) for the horizontal and (d) for the vertical component).

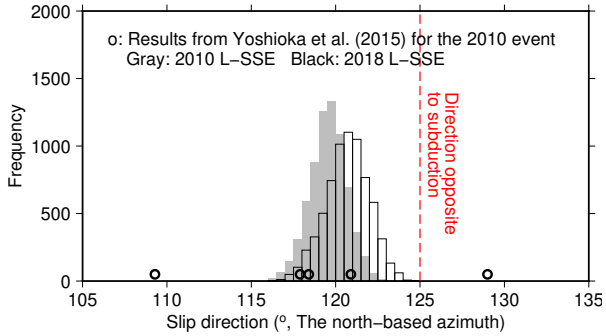

Figure S3. Histograms for the slip direction in the north-based azimuth calculated based on the rake deviation from the direction opposite to subduction (i.e., the 125° azimuth) estimated for the 2010 and 2018 L-SSE. The corresponding values in the five fault patches with the largest slip amount estimated by Yoshioka et al. (2015) for the 2010 L-SSE, denoted by black circles, are compared.

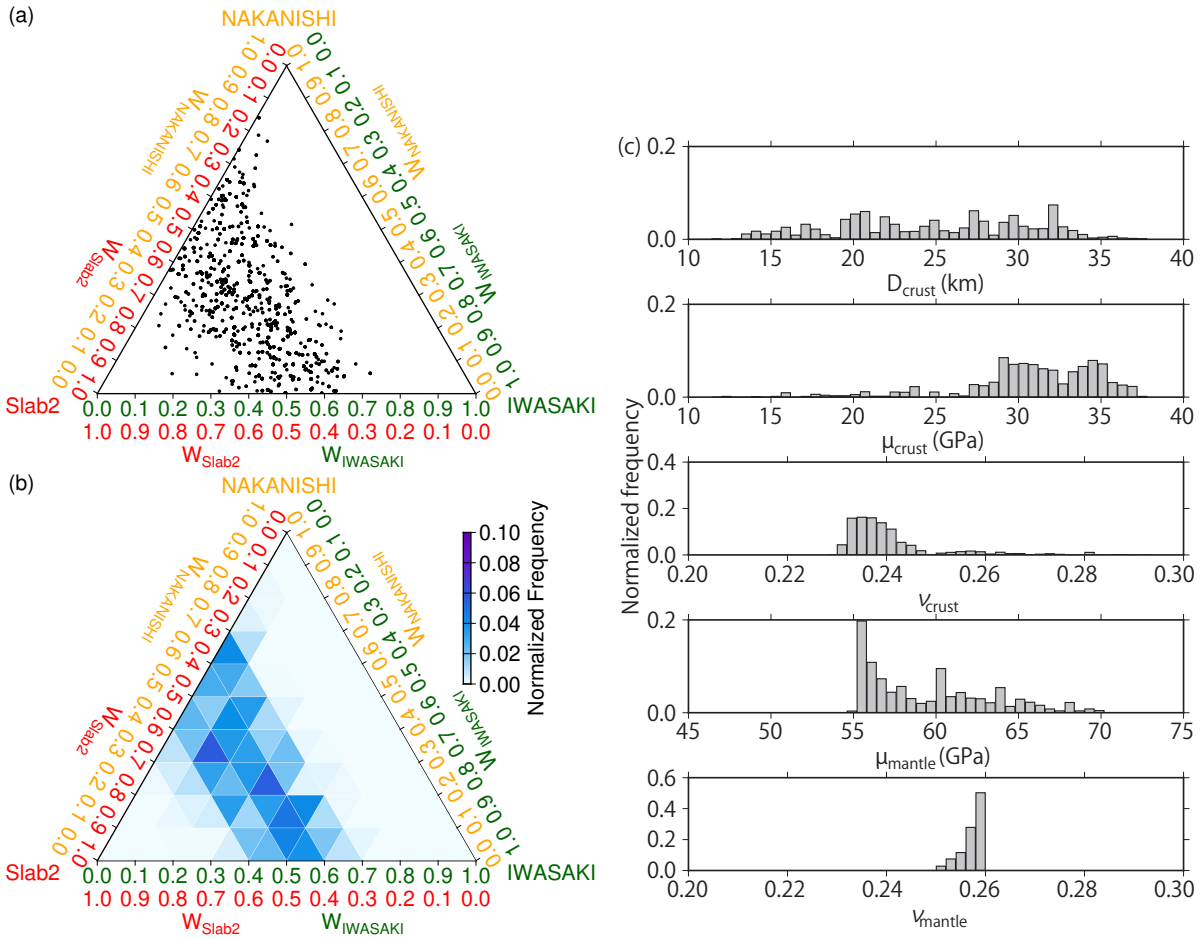

Figure S4. Samples for the prior PDF that are resampled from the samples obtained as the posterior PDF estimated for the 2010 L-SSE. (a) The plot ternary plot for the plate boundary geometry model using the dots. (b) That for the color map of normalized frequency in each small triangle. (c) The histograms for the elastic parameters.

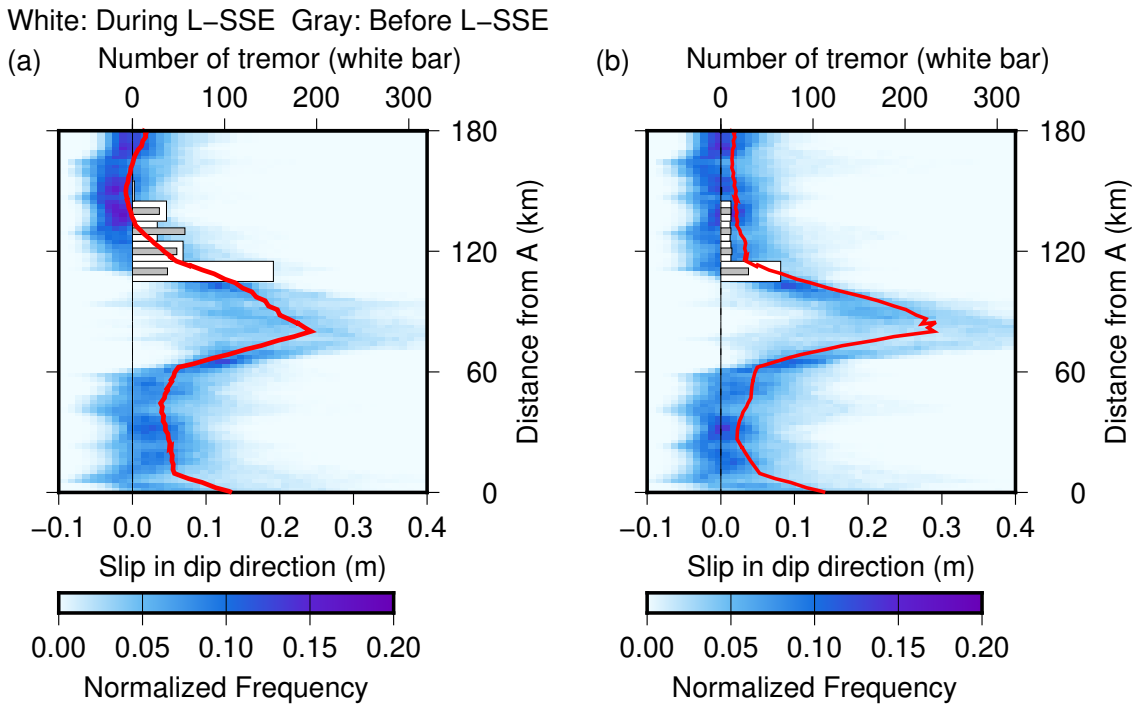

Figure S5. Comparison of the distribution of the number of tremor along the A-B line marked in Figure 10 and 11 before and during the period of L-SSE, which are denoted by the gray and white bars, respectively. (a) Those for the 2010 L-SSE. The tremors that occurred in a period between 2008.5 to 2009.5 are counted as "Before L-SSE", and the number of tremors counted here is scaled with the duration of the 2010 L-SSE for fair comparison. We do so because the occurrence of nearby S-SSEs has been reported in September 2008 (Kano et al., 2019) and it is necessary to consider its effect on the tremor occurrence. (b) Those for the 2018 L-SSE. The tremors that occurred in a period between 2018.3 to 2018.9 are counted as "Before L-SSE". The color map and the red line denote the frequencies of amount of slip for the posterior PDF and the mean slip distribution estimated by using BMMFSE, respectively.

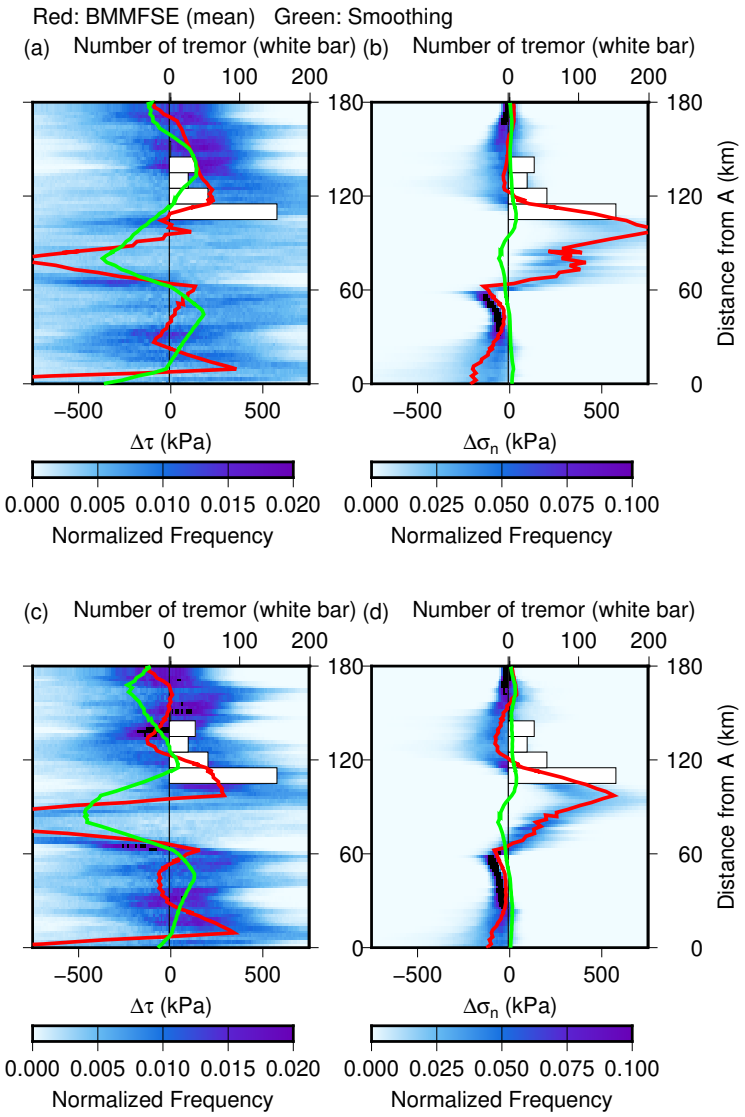

Figure S6. (a) Comparison of the distribution of $\Delta\tau$, the shear stress change on the fault, calculated using the posterior PDF for slip distribution for the 2010 L-SSE. The color map denotes the frequencies of $\Delta\tau$. The red and green line denote the distribution of $\Delta\tau$ of the mean of BMMFSE and the smoothing model, respectively. (b) Comparison of the distribution of $\Delta\sigma_{\mathrm{n}}$, the normal stress change on the fault, calculated using the posterior PDF for slip distribution for the 2010 L-SSE. The color map denotes the frequencies of $\Delta\sigma_{\mathrm{n}}$. The red and green line denote the distribution of $\Delta\sigma_{\mathrm{n}}$ of the mean of BMMFSE and the smoothing model, respectively. In all the figures, the white bars denote the number of tremors during the L-SSE period in the area within 5 km from the line in the direction perpendicular to it. (c)(d) Those for the 2018 L-SSE.

Table S1. Comparison of WBIC calculated in the estimation for the 2010 L-SSE with different grid spacings.

Grid spacing	12 km	14 km	16 km	18 km	20 km
WBIC	-1457.79	-1458.26	-1459.02	-1458.19	-1456.95